Nikolay Akatyev, Ruben Vardanyan, Ekaterina Kozhevnikova*

Faculty of Natural and Geographical Sciences, M.M.Utemisov West Kazakhstan University, Uralsk, Kazakhstan.

Scientific paper
ISSN 0351-9465, E-ISSN 2466-2585
https://doi.org/10.62638/ZasMat1694

Zastita Materijala 67 ()
(2026)

Experimental and theoretical investigation of NNO-type Schiff bases as corrosion inhibitors for carbon steel in 0.5 M H_2SO_4

ABSTRACT

This study investigates the corrosion inhibition performance of two NNO-type Schiff bases, namely (E)-2-(((pyridin-2-ylmethyl)imino)methyl)phenol (S1) and (E)-2-(phenyl((pyridin-2-ylmethyl) imino) methyl)phenol (S2), for carbon steel in 0.5 mol·dm^{-3} H_2SO_4 using both experimental and theoretical approaches. Weight loss measurements demonstrated high inhibition efficiencies for both compounds, with S2 exhibiting markedly greater performance, reaching a maximum efficiency of 91.19% at higher temperatures and concentrations. Adsorption studies revealed a mixed-type adsorption mechanism that follows the Langmuir isotherm model, with thermodynamic parameters indicating spontaneous and strong adsorption. Quantum chemical calculations provided insight into the electronic characteristics responsible for inhibition, highlighting the greater electronic stability and adsorption potential of S2. Molecular dynamics (MD) simulations confirmed stronger binding of S2 to the Fe(110) surface, with more favorable interaction pathways. Fukui function analysis further identified the key nucleophilic and electrophilic centers responsible for surface interactions, supporting the proposed inhibition mechanism.The results suggest that S2 is a more effective corrosion inhibitor due to its favorable electronic structure and stronger interaction with the metal surface.

Keywords: *Schiff bases, corrosion inhibitors, DFT, molecular dynamics, Fukui functions, adsorption.*

1. INTRODUCTION

Corrosion is a widespread phenomenon which causes significant material losses and compromises the structural integrity of metal components [1]. Among the various corrosion mitigation strategies, the use of organic inhibitors has proven particularly effective in acidic environments. The efficiency of organic inhibitors is closely associated with the presence of electron-donating functional groups and heteroatoms such as nitrogen, oxygen, and sulfur, as well as π-electron systems, which promote strong donor–acceptor interactions with the vacant *d*-orbitals of metal atoms [2]. Among the diverse array of organic compounds, Schiff bases constitute a particularly promising class of corrosion inhibitors [3,4]. This is primarily attributed to the presence of imine groups (–C=N–) and various heteroatoms, which provide multiple active sites for adsorption onto metal surfaces.

Their molecular architecture facilitates the formation of stable protective films while also allowing for the fine-tuning of physicochemical properties to suit specific conditions [5,6]. Functioning as mixed-type inhibitors, they effectively suppress both anodic and cathodic processes. This dual-action behavior is supported by their strong adsorption capabilities, which involve both physisorption and chemisorption mechanisms [7]. For instance, Schiff bases derived from 3-amino-1,2,4-triazole have been effective for carbon steel in acidic media, with efficiencies exceeding 90% [8], as well as aminopyridine-derived Schiff bases [9]. Schiff bases bearing naphthalene moieties have shown inhibition efficiencies (89%) in acidic media, confirmed by quantum chemical calculations [10].

Herein, the inhibitory properties of NNO-type Schiff bases have been studied using an experimental and theoretical approach. The primary novelty of this work lies in the combined theoretical and experimental investigation, as well as the comparative evaluation, of two specifically designed NNO-type Schiff bases, introduced here for the first time in this context. Although numerous Schiff bases have been extensively investigated

*Corresponding author: Nikolay Akatyev
E-mail: n.akatyev.science@gmail.com
Paper received: 24. 12. 2025.
Paper corrected: 23. 04. 2026.
Paper accepted: 15. 05. 2026.

using both experimental and theoretical approaches, the specific molecular architectures of S1 and S2 are novel and have not previously been reported or examined for this particular application.

2. EXPERIMENTAL DETAILS

NNO-type Schiff bases were synthesized from 2-(aminomethyl) pyridine, salicylic aldehyde and 2-hydroxyacetophenone as described in the literature without any modifications [11].

Carbon steel specimens (ST3SP2-GP2), with a composition of (wt.%) 97.75 Fe, 0.22 C, 0.65 Mn, 0.30 Si, 0.04 P, 0.05 S, 0.30 Cr, 0.30 Ni, 0.30 Cu, 0.01 N, and 0.08 As, and dimensions of 25.0 × 35.0 × 3.0 mm, were prepared for the corrosion experiment as we previously reported [12]. The corrosion rate (CR, g·m²·h⁻¹), inhibition efficiency (IE, %), and degree of surface coverage (θ) were calculated using Equations 1-3, respectively [13]:

$$CR(g \cdot m^{-2} \cdot h^{-1}) = \frac{\Delta m}{S \cdot \tau} \quad (1)$$

$$IE(\%) = \frac{CR_0 - CR_i}{CR_0} \quad (2)$$

$$\theta = \frac{IE(\%)}{100} \quad (3)$$

where Δm (g) represents the weight loss of the carbon steel specimen after an immersion period of τ (h), S (m²) is the surface area of the specimen, CR_0 denotes the corrosion rate of carbon steel in the absence of an inhibitor, and CR_i is the corrosion rate in the presence of the inhibitor.

In our study, the Langmuir adsorption model was applied to describe the adsorption of NNO-Schiff bases onto the carbon steel surface (4):

$$\frac{C_{inh}}{\theta} = \frac{1}{K_{ads}} + C_{inh} \quad (4)$$

where C_{inh} (mol·dm^{-3}) represents the inhibitor concentration, θ is the degree of surface coverage, and K_{ads} is the adsorption-desorption equilibrium constant. The values of K_{ads} obtained from the isotherms were used to evaluate the Gibbs free energy according to the known relationship (5):

$$\Delta G^0_{ads} = -RTIn(55.5K_{ads}) \quad (5)$$

where ΔG_{ads} is the Gibbs free energy of adsorption, R is the universal gas constant, T is the thermodynamic temperature, and 55.5 is the molar concentration of water (mol·dm^{-3}).

All quantum chemical calculations were carried out using the GAMESS software [14]. Initial geometry optimization was performed using the Molecular Mechanics (MM+) force field and then refined using the semi-empirical PM3 method. Final geometry optimizations and evaluations of quantum chemical parameters were conducted using Density Functional Theory (DFT) with the B3LYP functional employed in conjunction with the 6-311G+(d,p) basis set. All DFT calculations were carried out in both gas and aqueous phases. Solvent effects (H_2O) were modelled using the Conductor-like Screening Model (COSMO) [15].

The interaction between the investigated inhibitor and the metal surface was analyzed using molecular dynamics (MD) simulations with the GROMACS 2020.4 software package [16].

The adsorption energy was determined according to Equation (6):

$$E_{adsorption} = E_{total} - (E_{Fe(110)+solution} + \\ + E_{inhibitor}) \quad (6)$$

where E_{total} represents system containing Fe (110) surface, solution and corrosion inhibitor molecule.

The binding energy is regarded as the reciprocal of the adsorption energy of the inhibitor molecule as follows (7):

$$E_{bind} = -E_{adsorption} \quad (7)$$

Electrochemical measurement

The Autolab PGSTAT 101 Metrohm potentio stat/galvanostat, equipped with the NOVA 2.1.8 software, was used for the electrochemical test. A three-electrode setup was used for electrochemical measurements: a reference electrode (Ag/AgCl filled with 3.0 mol·dm⁻³ KCl), a counter electrode (platinum), and a working electrode (carbon specimen). A beaker containing 100 ml of corrosion medium, both with and without inhibitor, served as the electrochemical cell. The working electrode, with an exposed area of 1.00 cm², was stabilized during open circuit potential (OCP) testing. The linear sweep voltammetry (LSV) staircase and corrosion rate analysis were used to perform linear polarization measurements immediately after the OCP. Potentiodynamic scanning was performed with a scan rate of 0.01 V·s⁻¹ between -0.50 and +0.50 V. From the Tafel polarization curves, the corrosion potential (E_{corr}) and corrosion current density (j_{corr}) were established.

Equation 8 was used to obtain the inhibition efficiency (IE*i*%) through the corrosion current density:

$$IE_i(\%) = \frac{i_{inh} - i_{corr}}{i_{inh}} \quad (8)$$

where i_{inh} and i_{corr} are the corrosion current densities determined by extrapolating the Tafel slopes with and without inhibitors, respectively, in A·cm^{-2}.

Using the equation (9), the inhibition efficiency through the polarization resistance (IE_R%) was determined:

$$IE_R(\%) = \frac{R_p^{inh} - R_p^0}{R_p^{inh}} \quad (9)$$

where R_p^{inh} and R_p^0 represent the charge transfer resistance with and without an inhibitor, respectively, in Ω.

The reported results represent the mean of three independent experiments, with variability expressed as standard deviation (±SD) at a confidence probability of 0.95.

3. RESULTS AND DISCUSSION

Figure 1 illustrates the results of weight-loss experiments carried out with the inhibitor concentration range of $1 \cdot 10^{-3}$ – $1 \cdot 10^{-4}$ mol·dm^{-3} at 298 and 313 K for 18 h of exposure in 0.5 mol·dm^{-3} H_2SO_4.

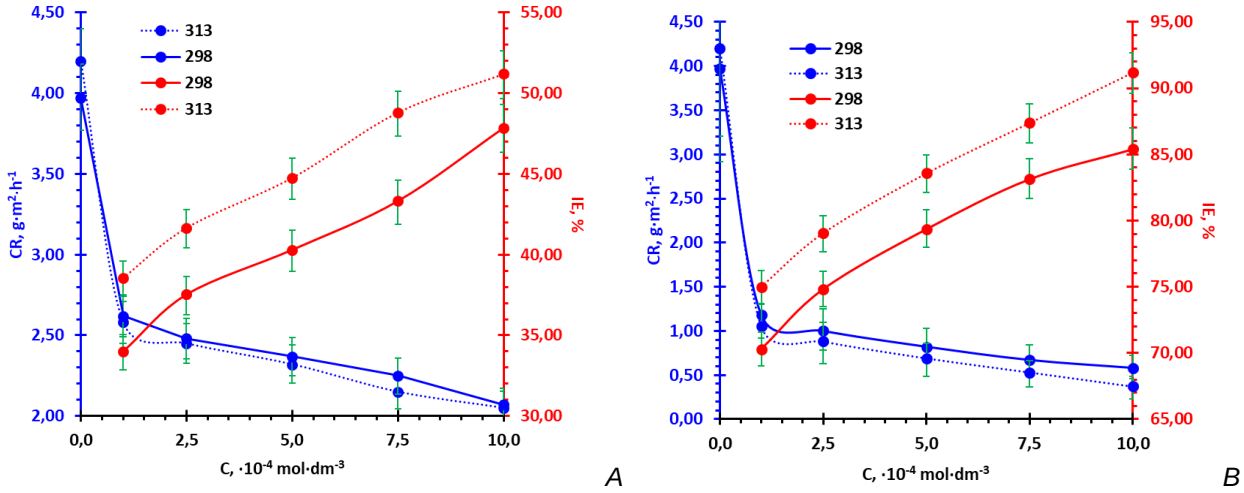

Figure 1. The relationship between CR (blue lines) and IE (red lines) on carbon steel in 0.5 mol·dm^{-3} H_2SO_4 solution and inhibitor concentration at 298 (solid lines) and 313 K (dashed lines) for S1 (A), S2 (B)

Figure 1 demonstrates that even low concentrations of both inhibitors lead to a pronounced reduction in the corrosion rate. The results further indicate that the NNO-type Schiff bases exhibit enhanced inhibition performance at elevated temperatures. The highest inhibition efficiency (91.19%) was achieved for S2 at the maximum investigated concentration ($1 \cdot 10^{-3}$ mol·dm^{-3}) and an elevated temperature of 313 K. Notably, S2 consistently exhibited approximately two-fold higher inhibition efficiency than S1 across the entire concentration range at both investigated temperatures.

Figure 2 presents the Langmuir adsorption isotherms [17] and thermodynamic parameters of adsorption of the NNO-Schiff bases on carbon steel surface in 0.5 mol·dm^{-3} H_2SO_4, at different temperatures.

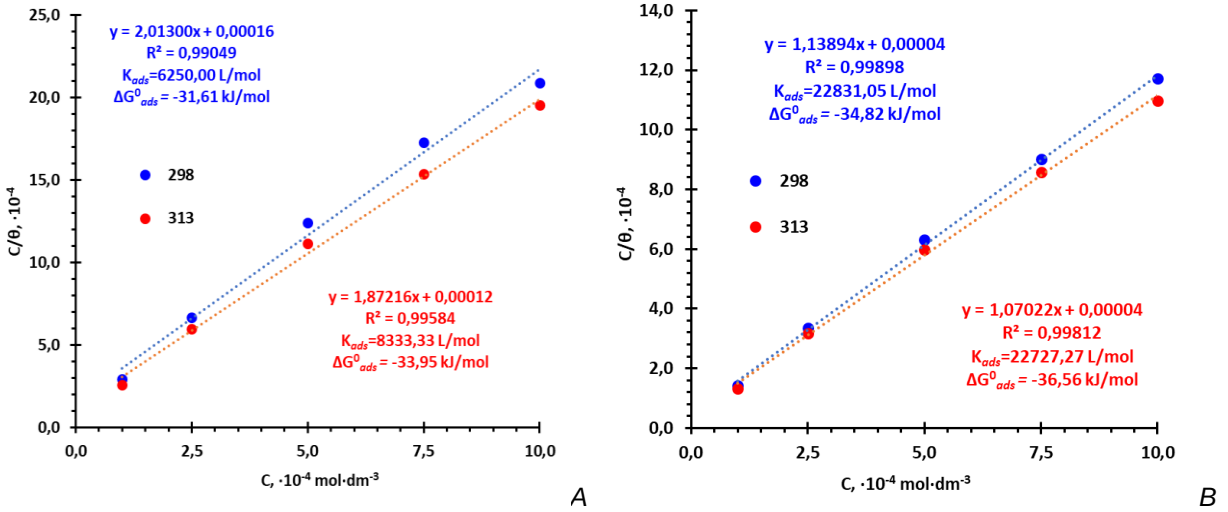

Figure 2. Langmuir adsorption isotherms and thermodynamic parameters of S1 (A) and S2 (B) in 0.5 mol·dm^{-3} H_2SO_4 solution at 298 K and 313 K

The excellent linearity of the C/θ *versus* C plots at both temperatures (R^2> 0.99) confirms that the adsorption of the NNO-Schiff bases follows the Langmuir isotherm. The negative values of ΔG^0_{ads} demonstrate that the adsorption process is spontaneous. A ΔG^0_{ads} value of approximately −35 kJ·mol^{-1} suggests strong adsorption of a mixed physisorption–chemisorption type, which is characteristic of azo-containing compounds. Moreover, the obtained results imply that the inhibitors form a monolayer coverage on the metal surface and that lateral interactions between the adsorbed molecules are negligible.

To elucidate the adsorption mechanisms in detail, experimental findings are often complemented by quantum chemical calculations [18]. Accordingly, in the present study, such calculations were performed to investigate the electronic properties and adsorption behavior of the studied compounds [19]. Figure 3 presents the molecular electrostatic potential (MEP) surfaces, frontier molecular orbital (HOMO and LUMO) distributions, and energy gap values (ΔE_{gap}) calculated with the DFT/B3LYP/6-311+G(d,p) level of theory.

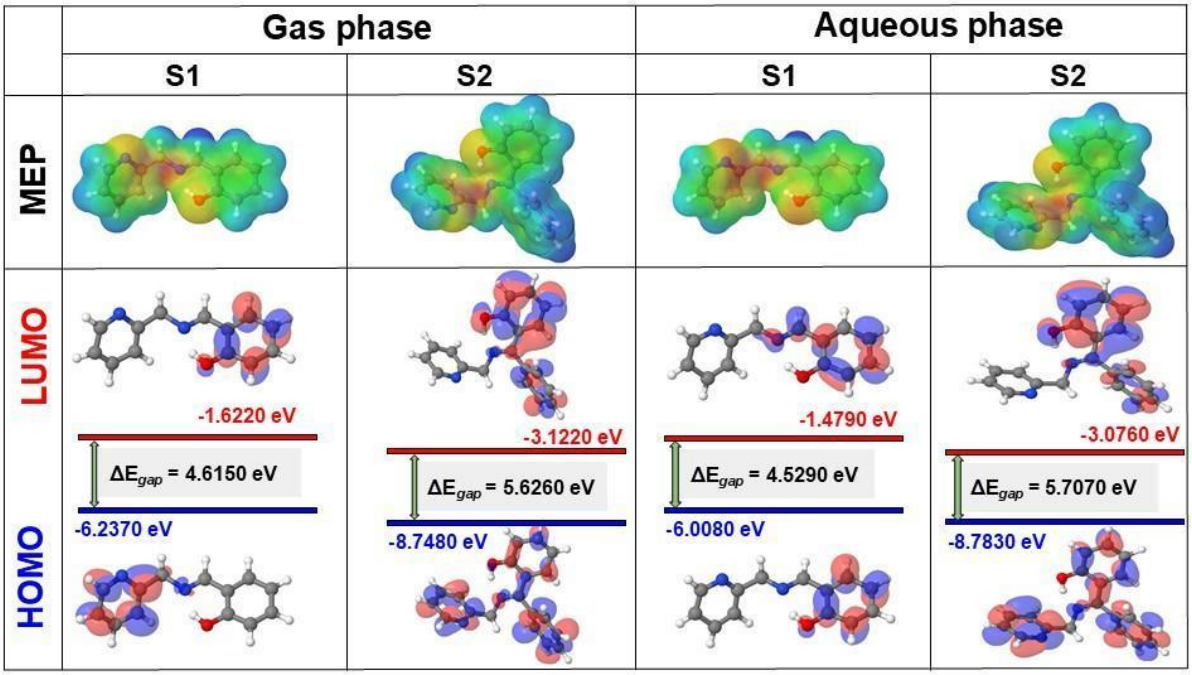

Figure 3. MEP, HOMO-LUMO energies and density distribution and energy gap (ΔE_{gap}) for NNO-Shiff bases calculated with DFT/B3LYP/6-311+G(d,p) level of theory

The frontier molecular orbital (FMO) analysis offers crucial insight into the electronic interactions governing inhibitor adsorption on the metal surface. As shown in Figure 3, the HOMO of S2 is predominantly localized over heteroatoms (N and O) and conjugated aromatic regions, indicating a strong electron-donating capability toward the vacant *d*-orbitals of the metal. This enhanced donor character facilitates chemisorptive contributions to adsorption. In contrast, the HOMO of S1 is more delocalized and less concentrated on active adsorption centers, implying a reduced ability to donate electrons and form strong surface interactions. The LUMO distribution of S2 is also more spatially accessible near heteroatom-rich regions, favoring back-donation from the metal surface and further stabilizing the adsorbed state. The HOMO–LUMO energy gap (ΔE_{gap}) provides an additional descriptor of molecular reactivity and stability. In both gas and aqueous phases, S2 exhibits a higher ΔE_{gap} compared to S1, indicating enhanced electronic stability of the inhibitor molecule after adsorption. This larger gap suggests lower susceptibility to electronic excitation and structural perturbation, favoring the formation of a more stable and persistent protective layer on the metal surface. Therefore, the combined effects of favorable frontier orbital localization and increased electronic stability, as reflected by the larger ΔE_{gap}, provide a clear theoretical rationale for the experimentally observed high corrosion inhibition performance of S2 relative to S1.

The molecular electrostatic potential (MEP) maps provide direct insight into the charge distribution and potential adsorption sites of the investigated inhibitors. As illustrated in Figure 3, regions of negative electrostatic potential (red/yellow) are predominantly localized around the heteroatoms (N and O), indicating electron-rich sites capable of interacting with positively charged metal surface atoms. Compared to S1, S2 shows more intense and spatially extended negative potential regions, especially around the functional groups containing azomethine nitrogen and oxygen. This effect is maintained in the water phase, which indicates that the solvent effects do not significantly interfere with the charge location in S2. Such well-defined electron-rich regions enhance electrostatic attraction and facilitate stronger adsorption of S2 onto the metal surface. In contrast, the MEP of S1 shows a more dispersed and less intense distribution of negative potential, suggesting weaker electrostatic interactions and lower surface affinity. Therefore, the MEP analysis also corroborates the experimental findings by indicating that S2 possesses more favorable electrostatic characteristics for stable and effective adsorption.

Furthermore, a number of global reactivity descriptors have been calculated to provide a more detailed view of the electronic properties and reactivity of the compounds studied. The results are summarized in Table 1.

Table 1. Calculated global reactivity descriptors for S1 and S2 in gaseous and aqueous phase

Descriptors	S1		S2	
	gas	aqueous	gas	aqueous
Total energy (E_{tot}), a.u.	-687.09	-687.09	-918.03	-918.02
Dipole moment (μ), D	1.6424	1.7302	1.9639	1.9728
Ionization energy (IP), eV	6.2370	6.0080	8.7480	8.7830
Electron affinity (EA), eV	1.6220	1.4790	3.1220	3.0760
Electronegativity (χ), eV	3.9295	3.7435	5.9350	5.9295
Chemical hardness (η), eV	2.3075	2.2645	2.8130	2.8535
Chemical softness (σ), eV	0.4334	0.4416	0.3555	0.3504
Electrophilicity index (ω), eV	7.7205	7.0069	17.6121	17.5795
Nucleophilicity index (ε), eV	0.1295	0.1427	0.0568	0.0569
Back-donation energy ($E_{b\text{-}d}$, eV)	-0.5769	-0.5661	-0.7033	-0.7134
Fraction of transferred electrons (ΔN)	-0.6653	-0.7190	-0.1890	-0.1875

Calculated quantum chemical descriptors confirm that S2 has a high corrosion-inhibiting potential in the aqueous phase. Its higher dipole moment (1.9728 D) favors adsorption on polar metal surfaces, while elevated ionization energy (8.7830 eV) and electron affinity (3.0760 eV) indicate electronic stability and strong electron-accepting ability. Greater electronegativity (5.9295 eV) further supports electron attraction during metal interaction. S2 shows higher chemical hardness (2.8535 eV vs. 2.2645 eV for S1), implying enhanced stability and long-term inhibition, consistent with its lower softness (0.3504 eV) and nucleophilicity (0.0569 eV). Its high electrophilicity (17.5795 eV) and more negative back-donation energy (-0.7134 eV) suggest stronger electron acceptance and stable adsorption. Minimal charge transfer (ΔN = -0.1875) also favors stable inhibitor–metal complexation. These descriptors highlight S2's electronic and adsorption properties, making it a more effective inhibitor than S1.

The Fukui function analysis was performed to identify the most reactive atomic sites involved in electron donation, electron acceptance, and radical interactions, which are directly relevant to the adsorption behavior of the inhibitors on the metal surface. The Fukui indices f^+, f^-, and f^0, which correspond to the electrophilic, nucleophilic, and radical attack centers were calculated using the finite-difference method [20]. The Fukui functions for the NNO-Schiff bases are presented in Figure 4.

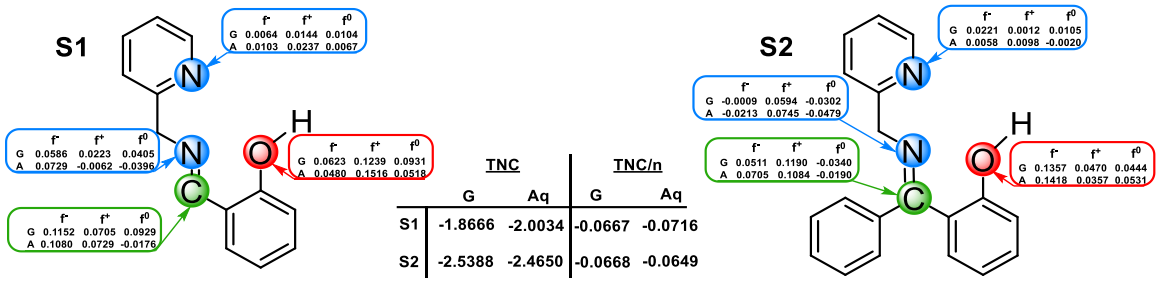

Figure 4. The Fukui functions of NNO-type Schiff bases calculated with DFT/B3LYP/6-311+G(d,p) method (only possible reactivity centers are marked for clarity)

As can be seen, for both S1 and S2, the nucleophilic Fukui indices (f^-) are predominantly localized on the heteroatoms, particularly the azomethine nitrogen and oxygen atoms, indicating that these sites are the primary electron-donating centers toward the vacant *d*-orbitals of the metal surface. Notably, S2 exhibits significantly higher f^- values at the oxygen and imine-related sites compared to S1, reflecting an enhanced electron-donating capability and stronger interaction potential with the metal. The electrophilic Fukui indices (f^+), which describe the tendency of a site to accept electrons, are also more pronounced for S2 at the same heteroatomic centers. This suggests that S2 can more effectively participate in back-donation interactions from the metal surface, contributing to the stabilization of the adsorbed inhibitor–metal complex. In contrast, S1 shows lower and more dispersed f^+ values, indicating weaker electrophilic responsiveness. The radical Fukui indices (f^0) further support these observations, as S2 presents higher absolute f^0 values at key adsorption centers, implying greater overall chemical reactivity and adaptability upon adsorption. This balanced distribution of nucleophilic and electrophilic reactivity in S2 favors the formation of a more stable and compact protective film on the metal surface. Furthermore, the TNC and TNC/n values show more negative values for S2 in both gas and aqueous phases, confirming its higher reactivity, which are favorable for adsorption-driven corrosion inhibition.

In summary favorable frontier orbital alignment, enhanced electronic stability, and stronger localized reactivity indices provide a clear theoretical explanation for the more significant corrosion inhibition performance of S2 compared to S1.

In addition, molecular dynamics simulations were carried out to assess the adsorption properties of NNO-Schiff bases on the surface of Fe(110). Figure 5 shows the proposed adsorption mechanism supported by top and bottom views of the most stable adsorption configurations of the two inhibitors, with their respective adsorption and binding energies.

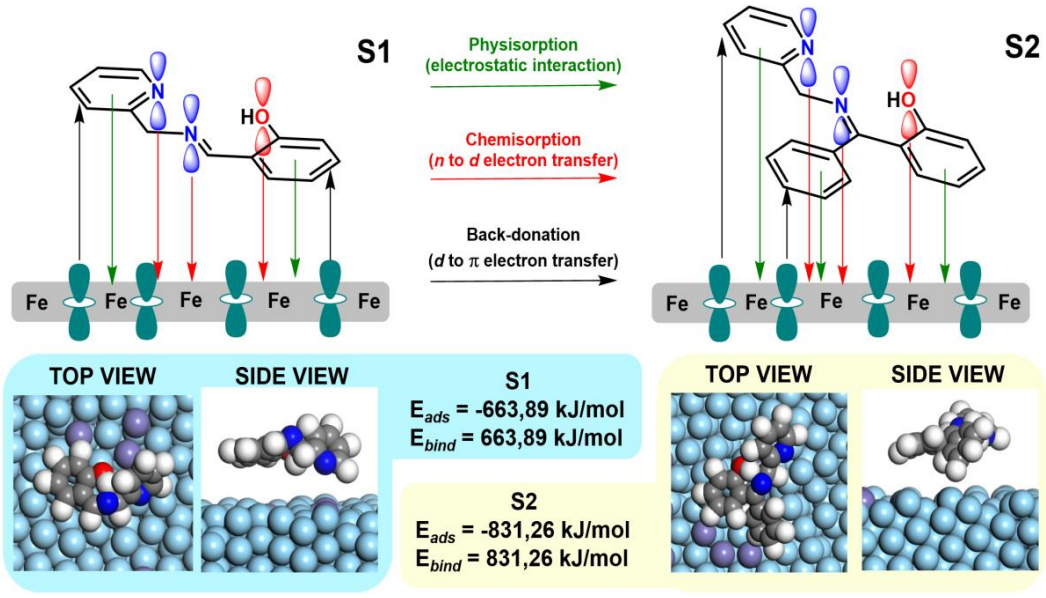

Figure 5. Proposed adsorption mechanism, MD-optimized configurations, interaction pathways, and adsorption energies of NNO-Schiff bases on the Fe (110) surface (water molecules were removed for clarity)

Figure 5 illustrates that the adsorption of the NNO-Schiff bases on the Fe(110) surface proceeds through a combination of physisorption, arising from electrostatic interactions between dipolar functional groups and the metal surface, and chemisorption, involving charge transfer from N and O lone pairs to vacant Fe d-orbitals, accompanied by stabilizing Fe→π back-donation. Molecular dynamics simulations show that both S1 and S2 adopt a nearly parallel adsorption orientation, which maximizes surface coverage and donor–surface interactions, with azomethine nitrogen and hydroxyl oxygen atoms positioned in close proximity to surface Fe atoms, in agreement with the Fukui function analysis. Notably, S2 exhibits a more favorable adsorption configuration, in which the spatial arrangement of donor atoms and extended π-conjugation enhance π–d orbital overlap and strengthen metal–inhibitor interactions. This is reflected in its more negative adsorption energy and higher binding strength compared to S1, confirming stronger and more thermo dynamically stable adsorption. Consequently, the MD-derived adsorption energies and geometries provide a clear molecular-level explanation for the superior corrosion inhibition efficiency of S2. Obtained results collectively indicate that both Schiff bases adsorb spontaneously and robustly on Fe(110) through mixed physisorption and chemisorption mechanisms, while the increased stability and surface affinity of S2 elucidate its consistently higher inhibition efficacy, aligning with experimental findings and quantum chemical descriptors.

Electrochemical results

The electrochemical behavior of carbon steel in 0.5 mol·dm^{-3} H_2SO_4 solution, both in the absence and presence of different concentrations of the NNO-Schiff bases, is depicted in Figure 6.

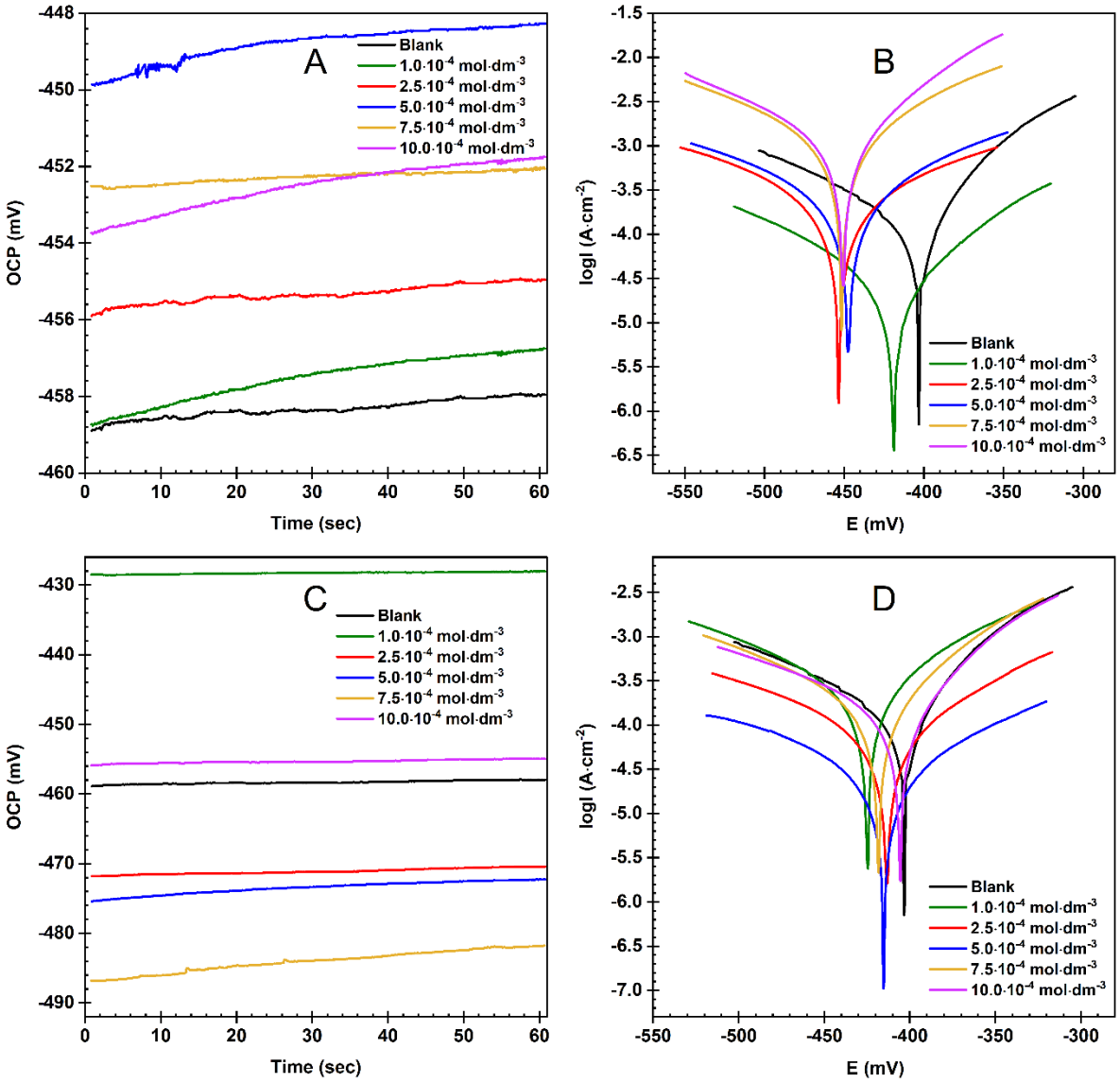

Figure 6. OCP vs. time diagrams (S1 – A, S2 - C) and Tafel polarization curves (S1 – B, S2 - D) for carbon steel in 0.5 mol·dm^{-3} H_2SO_4 solution with and without NNO-Schiff bases at room temperature

The electrochemical parameters of carbon steel in 0.5 mol·dm^{-3} H_2SO_4 in the absence and presence of various concentrations of NNO-Schiff bases derived from the polarization curves are summarized in Table 2.

Table 2. The electrochemical corrosion parameters of carbon steel in 0.5 mol·dm^{-3} H_2SO_4 in the absence and presence of different concentrations of NNO-Schiff bases

Concentration, 10^{-4} mol·dm^{-3}	-E_{corr}, mV	i_{corr}, $\cdot10^{-4}$ A·cm^{-2}	IE$_i$, %	|b_a|, mV·dec^{-1}	|b_c|, mV·dec^{-1}	R_p, Ω	IE$_R$, %
0.0	458.16 ± 8.43	18.23± 0.11	-	51.97	55.48	9.13± 0.36	-
S1							
1.0	488.42± 8.59	17.71± 0.21	2.85	66.62	92.46	10.89± 0.45	19.28
2.5	480.95± 7.55	16.43± 0.16	9.87	64.09	97.22	12.22± 0.51	33.84
5.0	472.33± 8.03	15.28± 0.11	16.18	63.07	93.06	13.45± 0.57	47.32
7.5	471.45± 7.71	14.24± 0.09	21.89	62.34	94.84	13.58± 0.62	48.74
10.0	470.99± 6.95	12.87± 0.11	29.40	65.09	91.18	14.14± 0.61	54.87

S2							
1.0	450.73± 7.09	9.65± 0.05	47.11	58.18	79.22	14.56± 0.69	59.47
2.5	451.15± 6.85	7.29± 0.04	60.02	58.19	68.36	15.01± 0.73	64.40
5.0	447.37± 6.56	5.99± 0.04	67.14	78.62	86.95	15.39± 0.76	68.57
7.5	453.35± 7.20	5.35± 0.03	70.67	68.31	65.99	15.82± 0.75	73.27
10.0	418.98± 6.62	4.56± 0.02	75.02	64.93	77.62	16.25± 0.81	77.98

Figure 6 presents the OCP-time profiles and Tafel polarization curves of carbon steel in 0.5 mol·dm^{-3} H_2SO_4 in the absence and presence of various concentrations of NNO-Schiff bases. In all cases, the OCP rapidly stabilizes, indicating the establishment of a steady electrochemical state. The addition of inhibitors shifts the OCP toward more noble potentials relative to the blank solution, reflecting the adsorption of inhibitor molecules and the formation of a protective film. The magnitude of this shift increases with inhibitor concentration, suggesting enhanced surface coverage. The Tafel polarization curves show a significant reduction in corrosion current density (i_{corr}) upon inhibitor addition. Both anodic and cathodic branches are suppressed, while the general shapes and slopes remain largely unchanged, indicating that the inhibitors reduce the corrosion rate without modifying the underlying electrochemical mechanisms. This behavior confirms that both S1 and S2 act as mixed-type inhibitors.

Increasing inhibitor concentration leads to a systematic decrease in i_{corr} and a concomitant increase in polarization resistance (R_p), consistent with progressive blockage of active corrosion sites. Inhibitor S1 provides moderate protection, whereas S2 exhibits substantially higher inhibition efficiency, exceeding 75% at the highest concentration studied. The high performance of S2 is attributed to its stronger adsorption and more effective surface coverage. The electrochemical results indicate that corrosion inhibition is governed by adsorption-controlled surface protection, with S2 exhibiting markedly higher inhibition efficiency than S1. These findings are in excellent agreement with the gravimetric measurements and theoretical calculations, which collectively confirm the superior inhibitory performance of S2 and demonstrate the robustness and internal consistency of the obtained results.

As a result, a unified inhibition mechanism can be established by correlating the experimental parameters, DFT descriptors, and MD simulations outcomes. Experimentally, the increase in inhibition efficiency with increasing temperature, together with moderately negative values of ΔG^0_{ads} and the predominance of Langmuir-type adsorption, indicates spontaneous adsorption governed mainly by physical interactions with a partial chemisorption contribution. This behavior is fully consistent with the DFT results, which reveal relatively high HOMO energies, narrow HOMO–LUMO gaps, and pronounced Fukui indices localized on the azomethine nitrogen and hydroxyl oxygen atoms, confirming the strong electron-donating capability and preferred adsorption sites of the inhibitors. These electronic features favor initial electrostatic attraction to the charged metal surface, followed by localized charge transfer interactions. Complementarily, MD simulations provide direct structural and energetic evidence, showing that both S1 and S2 adsorb in a nearly parallel orientation on Fe (110), maximizing surface contact and stabilizing the adsorbed layer through mixed physisorption–chemisorption mechanisms. The more negative adsorption energy and higher binding strength of S2 observed in MD simulations quantitatively support its larger adsorption equilibrium constant and superior inhibition efficiency obtained experimentally. In summary, the strong correlation between temperature-dependent adsorption behavior, DFT-derived reactivity descriptors and MD-predicted adsorption configurations confirm a coherent mechanism of inhibition, in which the molecular electronic structure controls the adsorption force, the surface stability and ultimately the corrosion protection properties.

4. CONCLUSION

The combined experimental and theoretical investigation confirms the strong anticorrosive potential of the studied NNO-type Schiff bases, with compound S2 exhibiting significant inhibitory performance. The corrosion inhibition efficiency was found to improve with increasing inhibitor concentration and temperature, indicating favorable thermally activated adsorption behavior. Thermodynamic analysis and isotherm modeling suggest a mixed adsorption mechanism involving both physisorption and chemisorption processes. Quantum chemical calculations at the B3LYP/6-311G+(d,p) level attribute the enhanced performance of S2 to its electronic structure – specifically, a larger HOMO–LUMO gap, localized electron density at key reactive centers, and the

presence of an additional aromatic ring that enhances surface interactions. Molecular dynamics simulations further validate these findings, demonstrating that S2 adopts a more favorable adsorption configuration on the Fe(110) surface and forms stronger interactions compared to S1. The consistency between theoretical predictions and experimental data highlights the robustness of the applied methodology. Generally, S2 emerges as a highly effective and promising corrosion inhibitor for carbon steel in acidic environments, offering a compelling combination of efficiency, structural advantages, and practical applicability.

5. REFERENCES

[1] C.-Q. Li, W. Yang, W. Shi (2020) Corrosion effect of ferrous metals on degradation and remaining service life of infrastructure using pipe fracture as example, Struct. Infrastruct. Eng., 16 (4), 583–598. https://doi.org/10.1080/15732479.2019.1663221

[2] A.A. Al-Amiery, W.N.R.W. Isahak, W.K. Al-Azzawi (2023) Corrosion Inhibitors: Natural and Synthetic Organic Inhibitors, *Lubricants*, 11(4), 174. https://doi.org/10.3390/lubricants11040174

[3] Q.A. Yousif, M.A. Bedair, A.M. Abuelela, A. Ansari, S.S. Malhotra (2025) Structure-activity relationship of some prepared Schiff bases as corrosion inhibitors for carbon steel in hydrochloric acid: Experimental and DFT insights, Mater. Today Commun., *49*, 113843. https://doi.org/10.1016/j.mtcomm.2025.113843

[4] Q.A. Yousif, A.A. Nazeer, Z. Fadel, L.A. Al-Hajji, K. Shalabi (2024) Design of new ecofriendly Schiff base inhibitors for carbon steel corrosion protection in acidic solutions: electrochemical, surface, and theoretical studies, ACS Omega, *9*(12), 14153–14173. https://doi.org/10.1021/acsomega.3c09688

[5] M.A. Bedair (2025) A Novel Coumarin-Azo Schiff Base for Dual Corrosion Inhibition for Steel in Acidic Environments and Anti-SRB Protection: Experimental and Computational Insights, Results Surf. Interfaces, 19, 100511. https://doi.org/10.1016/j.rsurfi.2025.100511

[6] N.B. Iroha, C.U. Dueke-Eze, V.C. Anadebe, N.J. Maduelosi, R. Thomas, E. E. Ebenso (2025) Assessment of a New Benzylidene-Based Corrosion Inhibitor for X60 Carbon Steel in 1 M HCl Medium: Experimental and Computational Studies, Results Surf. Interfaces, 19, 100510. https://doi.org/10.1016/j.rsurfi.2025.100510

[7] A. Lordjames, S.J. Temitope, A. D. Ojo, A. A. Adegalu. (2025). Schiff Bases as Effective and Sustainable Corrosion Inhibitors, Saudi J. Eng. Technol., 10 (4), 127–136. https://doi.org/10.36348/sjet.2025.v10i04.002

[8] E.A. Mohamed, A.A. Altalhi, A. Amer, N.A. Negm, E.A.M. Azmy, A.A. Farag (2023) Two Novel Schiff Bases Derived from 3-Amino-1,2,4-Triazole as Corrosion Inhibitors for Carbon Steel Pipelines during Acidizing Treatment of Oil Wells: Laboratory and Theoretical Studies, Energy Sources, Part A, 45 (2), 3246–3265. https://doi.org/10.1080/15567036.2023.2195817

[9] S.M. Al-Shomar, et al. (2025) Aminopyridine Schiff bases as eco-friendly corrosion inhibitors for carbon steel in acidic media: experimental and quantum chemical insights, J. Electrochem. Sci. Eng., *15* (4), 2769.https://doi.org/10.5599/jese.2769

[10] K. Pruthviraj, B.S. Chethan, N.K. Lokanath, S.V. Niranjana, N.N. Hebbar, K. Sunil (2024) Schiff Base Derived from 2-Hydroxy Napthaldehyde as Anti-Corrosive for Mild Steel in Acid Media: Experimental Investigation and Theoretical Modelling, Mol. Phys., 123 (4). https://doi.org/10.1080/00268976.2024.2385580

[11] J. Sun, T. Yu, H. Yu, M. Sun, H. Li, Z. Zhang, H. Jiang, S. Wang. (2014) Highly efficient turn-on fluorescence detection of zinc(ii) based on multi-ligand metal chelation,Anal. Methods, 6 (17), 6768–6773.https://doi.org/10.1039/C4AY00844H

[12] T. Seilova, Z. Kunasheva, R. Kubasheva, N. Akatyev (2024) Development of New Three-Component BNP-Inhibitor for Carbon Steel in 0.5 mol·dm^{-3} HCl Solution. Thermodynamic, Adsorption and Electrochemical Studies, Int. J. Corros. Scale Inhib., 13 (2). https://doi.org/10.17675/2305-6894-2024-13-2-33

[13] N.V. Akatyev, M.K. Khapieva, R.Zh. Kenzhegalieva, T.B. Seilova (2024) Black currant (*Ribes nigrum*) from Western Kazakhstan – a new natural environmentally friendly corrosion inhibitor for carbon steel, Vestn. Univ. Shakarima, Ser. Tekh. Nauki,1 2(14), 390–401. https://doi.org/10.53360/2788-7995-2024-2(14)-49

[14] M.W. Schmidt, K.K. Baldridge, J.A. Boatz, S.T. Elbert, M.S. Gordon, J.H. Jensen, J.A. Montgomery (1993) General atomic and molecular electronic structure system, J. Comput. Chem., 14 (11), 1347–1363. https://doi.org/10.1002/jcc.540141112

[15] A. Klamt (2017) The COSMO and COSMO-RS solvation models.WIREs Comput. Mol. Sci., *8* (1), e1338. https://doi.org/10.1080/15732479.2019.1663221

[16] Q.A. Yousif, Z. Fadel, A.M. Abuelela, E.H. Alosaimi, S. Melhi, M.A. Bedair (2023) Insight into the corrosion mitigation performance of three novel benzimidazole derivatives of amino acids for carbon steel (X56) in 1 M HCl solution, RSC Adv., *13*(19), 13094–13119. https://doi.org/10.1039/d3ra01837g

[17] Q.A. Yousif, M.A. Bedair, A.M. Abuelela, F. Al-Odail, A. Ansari, Z. Fadel (2025) Theoretical and experimental aspects of novel penicillanic acid compounds as corrosion inhibitors in acidic solutions,Mater. Today Commun., *47*, 113199. https://doi.org/10.1016/j.mtcomm.2025.113199

[18] Q.A. Yousif, M.A. Bedair, A.M. Abuelela, A. Ansari, S.S. Malhotra, Z. Fadel (2025) High-performance corrosion inhibitors for carbon steel in hydrochloric acid: electrochemical and DFT studies, RSC Adv.,*15* (35), 28666–28688. https://doi.org/10.1039/d5ra04952k

[19] M.J. Abraham, T. Murtola, R. Schulz, S. Páll, J.C. Smith, B. Hess, E. Lindahl (2015) GROMACS: High performance molecular simulations through multi-level parallelism from laptops to supercomputers,

SoftwareX, 1, 19-25. https://doi.org/10.1016/j.softx.2015.06.001
[20] Z. El Adnani, M. Mcharfi, M. Sfaira, M. Benzakour, A.T. Benjelloun, M.E. Touhami (2013) DFT theoretical study of 7-R-3methylquinoxalin-2 (1H)-thiones (RH; CH_3; Cl) as corrosion inhibitors in hydrochloric acid, Corr. Sci., 68, 223-230. https://doi.org/10.1016/j.corsci.2012.11.020

IZVOD

EKSPERIMENTALNO I TEORIJSKO ISTRAŽIVANJE ŠIFOVIH BAZA NNO TIPA KAO INHIBITORA KOROZIJE ZA UGLJENIČNI ČELIK U 0,5 M H_2SO_4

Ova studija istražuje performanse inhibicije korozije dve Šifove baze NNO tipa, naime (E)-2-(((piridin-2-ilmetil)imino)metil)fenola (S1) i (E)-2-(fenil((piridin-2-ilmetil)imino)metil)fenola (S2), za ugljenični čelik u 0,5 mol·dm^{-3} H_2SO_4 koristeći i eksperimentalne i teorijske pristupe. Merenja gubitka težine pokazala su visoku efikasnost inhibicije za oba jedinjenja, pri čemu S2 pokazuje znatno veće performanse, dostižući maksimalnu efikasnost od 91,19% na višim temperaturama i koncentracijama. Studije adsorpcije otkrile su mehanizam adsorpcije mešovitog tipa koji prati Langmirov izotermni model, sa termodinamičkim parametrima koji ukazuju na spontanu i jaku adsorpciju. Kvantno-hemijski proračuni pružili su uvid u elektronske karakteristike odgovorne za inhibiciju, ističući veću elektronsku stabilnost i adsorpcioni potencijal S2. Molekularno-dinamske (MD) simulacije potvrdile su jače vezivanje S2 za površinu Fe(110), sa povoljnijim putevima interakcije. Analiza Fukuijeve funkcije dodatno je identifikovala ključne nukleofilne i elektrofilne centre odgovorne za površinske interakcije, podržavajući predloženi mehanizam inhibicije. Rezultati ukazuju na to da je S2 efikasniji inhibitor korozije zbog svoje povoljne elektronske strukture i jače interakcije sa površinom metala.

Ključne reči: *Šifove baze, inhibitori korozije, DFT, molekularna dinamika, Fukuijeve funkcije, adsorpcija*

Naučni rad
Rad primljen: 24.12.2025.
Rad korigovan: 23.04.2026.
Rad prihvaćen: 15.06.2026.

Nikolay Akatyev: https://orcid.org/0000-0001-9248-2753,
Ruben Vardanyan: https://orcid.org/0009-0003-6291-8191,
Ekaterina Kozhevnikova: https://orcid.org/0009-0002-4406-827X,